

# Regge Trajectories of Meson Excitations in the Pseudo-scalar and Vector Channels: Exploring the Dyson-Schwinger – Bethe-Salpeter Approach

R. Greifenhagen,<sup>1</sup> B. Kämpfer,<sup>1,2</sup> and L. P. Kaptari<sup>2,3</sup>

<sup>1</sup>*Institut für Theoretische Physik, TU Dresden, 01062 Dresden, Germany\**

<sup>2</sup>*Helmholtz-Zentrum Dresden-Rossendorf, PF 510119, 01314 Dresden, Germany†*

<sup>3</sup>*Bogoliubov Lab. Theor. Phys., 141980, JINR, Dubna, Russia ‡*

The combined Dyson-Schwinger and Bethe-Salpeter equations in rainbow-ladder approximation are used to search for Regge trajectories of radially excited mesons in the pseudo-scalar and vector channels. We focus on the often employed Alkofer-Watson-Weigel kernel which is known to deliver good results for the ground state meson spectra; it provides linear Regge trajectories in the  $J^P = 0^-$  channel.

## I. INTRODUCTION

Despite of the apparent simplicity of the Lagrangian where Quantum Chromodynamics (QCD) is based upon, it encodes an enormous richness of phenomena, most of them related to the non-perturbative regime. While lattice QCD allows for an access to many facets of the hadron spectra, the so called XYZ states pose still a challenge [1]. Apart the quantitatively adequate description of low-lying hadron states in various flavor channels, the higher excitations call also for a description and confrontation with experimentally well established facts. It is known for a long time that mesons of a given flavor composition can be grouped on radial Regge trajectories according to  $M_n^2 = M_0^2 + n\mu^2$ , where  $M_n$  stands for the mass (energy) labeled by the radial quantum number  $n = 0, 1, 2, \dots$ ,  $M_0$  denotes the ground state mass of a respective trajectory and  $\mu^2 = 1.25 \text{ GeV}^2$  [2] or  $1.35 \text{ GeV}^2$  [3] is a universal slope parameter (cf. [3, 4] for a recent account and [5–8] for the discussion of the experimental data base). More generally, Ref. [9] advocates an ordering according to  $M_{n,J}^2 = \hat{a}(n + J) + \hat{c}$ , where  $J$  stands for the angular momentum and  $\hat{a}$  and  $\hat{c}$  are appropriate constants, see also [10]. Often, a grouping according to  $M_J^2 = M^2(0) + \hat{\beta}J$  is considered prototypically for a linear orbital Regge trajectory.

While being a phenomenological ordering scheme, the arrangement of hadron states on Regge trajectories should emerge from QCD, ideally directly without approximations or based on certain symmetries or as result of suitable models. In fact, the relativistic quark model [11, 12] delivers such linear trajectories. Also holographic models based on the AdS/CFT correspondence (cf. [6, 13]) cope with Regge trajectories [14], or even use them as input for constraining the dilaton dynamics for further investigations [15–17]. Moreover, functional formulations of QCD such as combined Dyson-Schwinger (DS) and Bethe-Salpeter (BS) equations address the issue of recovering Regge trajectories [18, 19] with appropriate interactions

---

\*Electronic address: r.greifenhagen@hzdr.de

†Electronic address: kaempfer@hzdr.de

‡Electronic address: kaptari@theor.jinr.ru

kernels and truncation schemes [20]. The latter approach is interesting since it provides the avenue towards addressing the important quest for medium modifications of hadrons in a hot and dense hadron medium [21]. Considering the medium created transiently in the course of relativistic heavy-ion collisions, the interplay of confinement and chiral symmetry restoration poses further challenges [22]. In this context, radial excitations of quarkonia play an important role as diagnostic tool: The relative strengths of  $\psi(2s)$  or  $\Upsilon(2s)$  states to  $J/\psi$  or  $\Upsilon(1s)$ , measured via their  $e^+e^-$  and  $\mu^+\mu^-$  decay channels, depend on the centrality in nucleus-nucleus collisions and are different in proton-nucleus as well as proton-proton collisions at LHC energies. This is interpreted as a hint to sequential meson melting of heavy vector states, further supported by the suppression of  $\Upsilon(3s)$  in heavy-ion collisions [23–27].

Here, we focus on the question whether the DS-BS approach in rainbow-ladder approximation is capable to deliver Regge type trajectories of radial excitations when using simple interaction kernels. To be specific we employ the Alkofer-Watson-Weigel (AWW) kernel [28] in the pseudo-scalar ( $J^P = 0^-$ ) and vector ( $J^P = 1^-$ ) channels and search for the first excited states. Such a study is a prerequisite for the extension to non-zero temperatures [29]. The AWW kernel is known to provide a good description of meson ground states supposed the analytic properties of the quark propagators are properly dealt with [30–32]. However, in the literature one finds remarks that AWW is less appropriate for a description of excitations due to their sensitivity to long-range interactions [20, 28, 33, 34] (for dedicated studies, cf. [35–39] for instance). Nevertheless, we feel that a further investigation is timely, in particular w.r.t. the above stressed importance of Regge trajectories as an important feature of the meson spectrum. For the search of meson excitations we employ a method, based on investigations of zeros of determinants of the corresponding system of homogeneous equations, to search for the radial excitations of the BS equation. In our approach, each value of the mass which zeroes out the determinant above the ground state is associated with one excited state on the  $0^-$  or  $1^-$  trajectory.

Our paper is organized as follows. In section 2 we recall the DS and BS equations as well as the AWW kernel. Numerical results are described in section 3. We summarize in section 4. The appendix contains some technicalities.

## II. RECALLING THE DS AND BS EQUATIONS IN RAINBOW-LADDER APPROXIMATION

The DS equation (also dubbed gap equation) aims at solving

$$S^{-1}(p) = S_0^{-1}(p) - \int \frac{d^4k}{(2\pi)^4} \left[ -ig^2\gamma^\nu\frac{\tau^a}{2} \right] \mathcal{D}_{\mu\nu}(p,k)\Gamma^{\mu,a}(p,k)S(k), \quad (1)$$

for the dressed quark propagator  $S$ , where  $S_0$  is the free quark propagator,  $\gamma^\nu$  are the Dirac matrices with  $\{\gamma^\mu, \gamma^\nu\} = 2\delta^{\mu\nu}$ ,  $\tau^a$  are color matrices,  $p$  and  $k$  are four-momenta,  $g$  is the QCD coupling constant, and  $\mathcal{D}_{\mu\nu}$  stands for the gluon propagator. In Euclidean space, the rainbow approximation consists in a replacement of the dressed quark-gluon vertex  $\Gamma^{\mu,a}(p,k)$  by the free one,  $\Gamma^{\mu,a}(p,k) \Rightarrow -i\gamma^\mu\frac{\tau^a}{2}$  and in a replacement of the exact interaction kernel  $g^2\mathcal{D}_{\mu\nu}(k)$  by the free propagator and a properly chosen form-factor  $D(k^2)$ , i.e.  $g^2\mathcal{D}_{\mu\nu}(k) \longrightarrow (\delta_{\mu\nu} - k_\mu k_\nu/k^2) D(k^2)$ , see below. The equation for the quark

propagator reads

$$S^{-1}(p) = S_0^{-1}(p) + \frac{4}{3} \int \frac{d^4 k}{(2\pi)^4} [g^2 \mathcal{D}_{\mu\nu}(p-k)] \gamma^\mu S(k) \gamma^\nu \quad (2)$$

with  $S_0^{-1}(p) = i\not{p} + m_q$ , where the parameter  $m_q$  is flavor dependent.

The dressed quark propagator  $S(p)$  enters the BS equation for the vertex function

$$\Gamma(P, p) = \int \frac{d^4 k}{(2\pi)^4} K(P, p, k) S(k + \eta_1 P) \Gamma(P, k) S(k - \eta_2 P), \quad (3)$$

where  $p$  and  $P$  are the total and relative momenta of quarks and  $\eta_1 + \eta_2 = 1$  describes momentum sharing  $P = (iM_{12}, \mathbf{0})$  (for a meson a mass  $M_{12}$  at rest), and the rainbow approximation for the kernel function

$$K(P, p, k) = -g^2 \mathcal{D}_{\mu\nu}(p-k) \left( \gamma^\mu \frac{\tau^a}{2} \right) \left( \gamma^\nu \frac{\tau^a}{2} \right). \quad (4)$$

In the Euclidean space, the used BS equation becomes then

$$\Gamma(P, p) = -\frac{4}{3} \int \frac{d^4 k}{(2\pi)^4} \gamma^\mu S(k + \eta_1 P) \Gamma(P, k) S(k - \eta_2 P) \gamma^\nu [g^2 \mathcal{D}_{\mu\nu}(p-k)]. \quad (5)$$

Note the complex valued momenta of quarks entering the BS equation (5). In the present paper, we employ the AWW kernel, i.e.  $D(k^2) \Rightarrow D^{\text{AWW}}(k^2)$  in the decomposition of the gluon propagator in Landau gauge,  $g^2 \mathcal{D}_{\mu\nu}(k) = (\delta_{\mu\nu} - k_\mu k_\nu k^{-2}) D(k^2)$  with

$$D^{\text{AWW}}(k^2) = \frac{4\pi^2 D k^2}{\omega^2} e^{-\frac{k^2}{\omega^2}}, \quad (6)$$

with the interaction strength parameter  $D$  and the interaction range parameter  $\omega$ . (In what follows, we employ  $\eta_1 = \eta_2 = 1/2$  and the standard model parameters  $\omega = 0.5 \text{ GeV}$  and  $D = 16 \text{ GeV}^{-2}$ , unless explicitly noted.) It is the IR part of the Maris-Tandy kernel [40]. Results for the AWW and Maris-Tandy kernels are compared in [19].

### III. NUMERICAL METHODS AND RESULTS

The numerical details for solving the above q uoted DS and BS equations with given truncations and approximations are described in [41]. In vacuum, the quark propagator can be decomposed as  $S^{-1}(p) = i\gamma \cdot p A(p) + B(p)$  to split (2) into two coupled integral equations for  $A$  and  $B$  which, as already mentioned, are needed for complex arguments  $p$ . The introduced functions  $A(p)$  and  $B(p)$  are referred to as the quark wave function and quark-mass parameter, respectively. The dynamically generated quark mass is then  $M_q^2 = (B(p)/A(p))^2$ . Figure 1 exhibits examples for these functions for positive, real values of the momentum  $p$ . Note the non-linear dependence on the quark mass parameter  $m_q$ .

Making an expansion of the BS vertex function (5) into spin-angular functions, spherical harmonics and Gegenbauer polynomials and performing the angular integration explicitly, and approximating the resulting one-dimensional integrals by a proper quadrature formula, one arrives at an algebraic system of equations in a matrix form  $X_\alpha = \hat{S}_{\alpha\beta} X_\beta$  with  $\alpha, \beta = 1, \dots, N$ , where  $N = \alpha_{\text{max}} N_{\text{Gegenbauer}} N_{\text{Gauss}}$ . Here,  $\alpha_{\text{max}}$  denotes the number of spin-angular harmonics,  $N_{\text{Gegenbauer}}$  is the number of included Gegenbauer

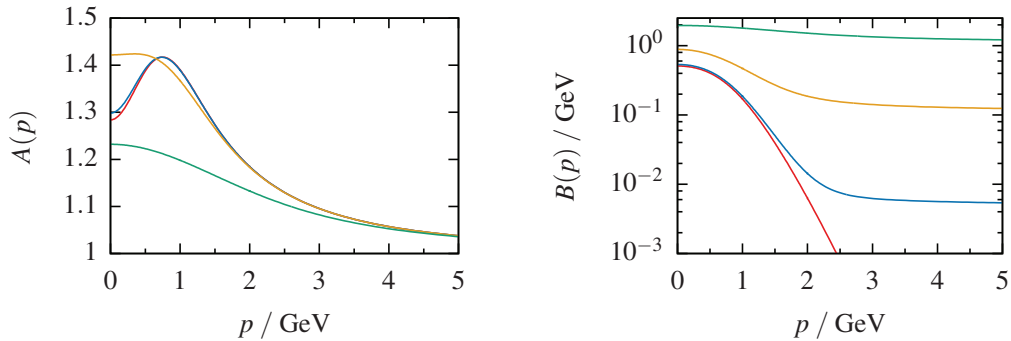


FIG. 1: (Color online) Propagator functions  $A(p)$  (left) and  $B(p)$  (right) on the positive real axis. Red curve:  $m_q = 0$  MeV (chiral limit), blue curve:  $m_q = 5$  MeV, yellow curve:  $m_q = 115$  MeV, green curve:  $m_q = 1130$  MeV.

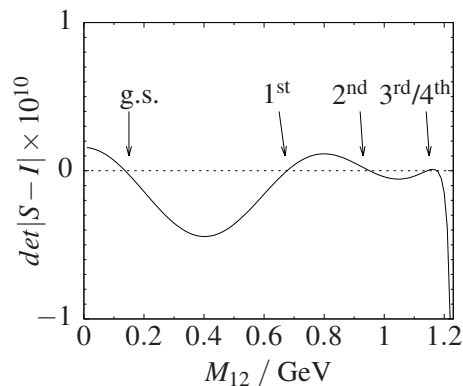


FIG. 2: Smooth determinant function  $\det(\hat{S} - \mathbb{1})$  as a function of  $M_{12}$  for the pion channel ( $m_{1,2} = m_q = m_u = 5$  MeV). For  $\omega = 0.3$  GeV and  $D = 205.761$  GeV $^{-2}$ . (These non-standard parameters have been chosen for the sake of a demonstration example which displays higher excitations.) The arrows denote the masses of ground state (g.s.), first excited state (1<sup>st</sup>), second excited state (2<sup>nd</sup>), third and fourth excited states (3<sup>rd</sup> and 4<sup>th</sup>).

polynomials, and  $N_{Gauss}$  stands for the mesh number of the employed quadrature formula (Gaussian integration mesh, in our case). The chain of manipulations that leads to the quantity  $\hat{S}_{\alpha\beta}$  is recalled in the Appendix, where also the elements of  $X$  are defined, see also Ref. [31] for details.

The energy of mesons as  $\bar{q}q$  bound states is determined by  $\det|\hat{S} - \mathbb{1}| = 0$  with  $\hat{S}$  being a function of the quantity  $M_{12}$  which appears in Eq. (15) in the Appendix. An example is exhibited in Fig. 2.

The AWW kernel depends on two parameters,  $D$  and  $\omega$ ; in addition the quark masses  $m_{1,2}$  ( $m_1 = m_2 = m_q$  for equal quark-mass mesons) must be adjusted. Figure 3 exhibits examples of meson ground state masses  $M_{n=0,J}(m_1, m_2)$  as contour plots over the  $m_1 - m_2$  plane for the pseudo-scalar (left,  $J = 0$ ) and vector (right,  $J = 1$ ) channels. One can select suitably three meson masses to determine, for given  $\{\omega, D\}$ , the  $m_{u/d,s,c}$  quark masses. For instance,  $M_{\rho,\phi,J/\psi}$  would be such a triple on the  $m_1 = m_2$  diagonal, see right panel, or include additionally a non-diagonal combination, such as  $K^*$ . A consistency check is provided by a comparison with quark masses delivered by the  $M_{\pi,K,\eta_c}$  mass values by an analog procedure, see left panel. The off-sets of the dashed horizontal lines in both panels point to a slight tension, i.e. one can not reproduce exactly the mentioned input meson masses at once for the given

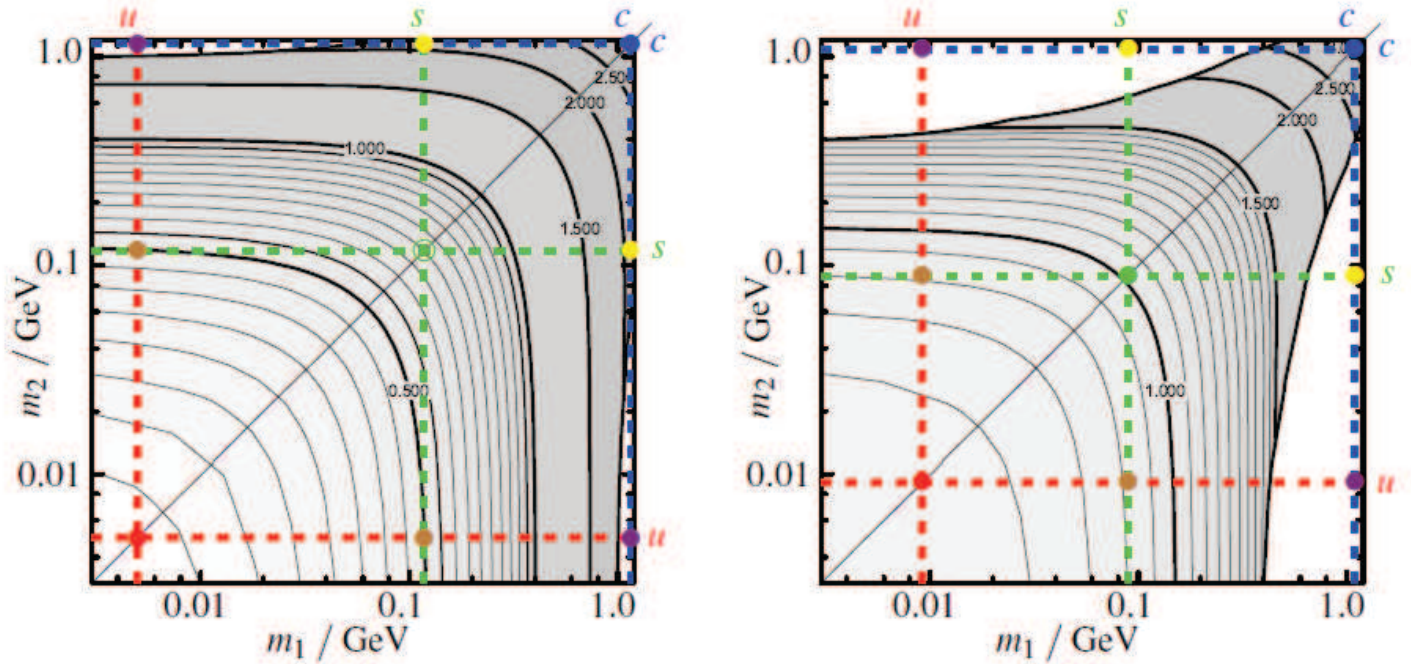


FIG. 3: (Color online) Contour plot of pseudo-scalar (left) and vector (right) meson ground state masses in units of GeV for varying quark masses  $m_1$  and  $m_2$ . The colored bullets denote the experimental values of meson ground states (red:  $\pi/\rho$ , green:  $K/\phi$ , violet:  $\eta_c/J_\psi$ ) which could be used for extracting the bare quark mass parameters  $m_{1,2}$  (vertical and horizontal dashed lines, labeled by the corresponding quark flavor). In the white region, no solutions of the BS equation could be found w/o accounting explicitly for the pole structure of  $S$  in the complex momentum plane.

interaction kernel parameters  $\{\omega, D\}$ . For instance, the corresponding value of  $m_c = 1.110$  GeV in the vector channel can be compared with one suggested in the pseudo-scalar channel, with optimum value 1.130 GeV etc.

In Table I, we present results of our calculations of the mass spectrum of ground states and excitations of a few first lightest pseudo-scalar ( $\pi$ ,  $K$ ,  $s\bar{s}$ ,  $D$  and  $\eta$ ) and vector ( $\rho$ ,  $K^*$ ,  $\phi$ ,  $D_s$  and  $J/\Psi$ ) mesons. Whenever possible, our results are compared with experimental data [42] and with calculations reported in [19]. The lack of corresponding information in Table I is denoted by "–". In addition, we note  $f_\pi = 0.133$  GeV and  $\langle \bar{q}q \rangle = (-0.255 \text{ GeV})^3$  [41]. The overwhelming impression is that, despite of the truncation and the simple interaction kernel, quite reasonable numbers for the ground states are delivered (most notable for  $\pi$ ,  $K$ ,  $D_s$ ,  $\eta_c$  in the  $0^-$  channel and  $\rho$ ,  $K^*$ ,  $\phi$ ,  $J/\psi$  in the  $1^-$  channel), however, with some drastic deviations, e.g. the pure pseudo-scalar  $\bar{s}s$  states do not appear in nature and our failure for  $D$ ,  $D^*$ ,  $D_s^*$  for the given parameters. (Employing the parameters of [43] we reproduce accurately the  $D$ ,  $D_s$  results reported there.) Improvements can be established, e.g. to use the full Maris-Tandy kernel and allow for a flavor dependent variation of the partition parameter  $\eta$  as in Ref. [18, 44]. The latter work includes many more channels from  $0^{-+}$  up to  $3^{++}$ . Focusing on the natural Regge trajectory sequence  $J^{PC} = 1^{--}, 2^{++}, 3^{--}$ , [18, 44] find a linear relationship  $M_J^2 = M^2(0) + \hat{\beta}J$  which is intriguing since the approach does not incorporate any linearly rising inter-quark potential. Due to our restriction on pseudo-scalar and vector channels we

	our results	results of	[19]	[42]		our results	results of	[19]	[42]
	$J^P = 0^-$	$J^{PC} = 0^{-+}$	$J^{PC} = 0^{--}$			$J^P = 1^-$	$J^{PC} = 1^{--}$	$J^{PC} = 1^{-+}$	
$M_{\pi, \text{g.s.}}$	0.137	0.137		0.140	$M_{\rho, \text{g.s.}}$	0.758	0.758		0.775
$M_{\pi, 1\text{st}}$	0.986		0.985		$M_{\rho, 1\text{st}}$	1.041	1.041		1.465
$M_{\pi, 2\text{nd}}$	1.369*			1.300	$M_{\rho, 2\text{nd}}$	1.064		1.062	
					$M_{\rho, 3\text{rd}}$	1.287*			1.720
$M_{K, \text{g.s.}}$	0.492	0.492		0.494	$M_{K^*, \text{g.s.}}$	0.945	0.946		0.894
$M_{K, 1\text{st}}$	1.162	1.162		1.460	$M_{K^*, 1\text{st}}$	1.264	–		1.414
$M_{s\bar{s}, \text{g.s.}}$	0.693	0.693			$M_{\phi, \text{g.s.}}$	1.077	1.078		1.019
$M_{s\bar{s}, 1\text{st}}$	1.278		1.278		$M_{\phi, 1\text{st}}$	1.402		1.400	
$M_{s\bar{s}, 2\text{nd}}$	1.572*				$M_{\phi, 2\text{nd}}$	1.430	1.428		1.680
					$M_{\phi, 3\text{rd}}$	1.598*			2.175
$M_{D, \text{g.s.}}$	–	–		1.870	$M_{D^*, \text{g.s.}}$	–	–		2.010
$M_{D_s, \text{g.s.}}$	2.075	2.041 <sup>#</sup>		1.968	$M_{D_s^*, \text{g.s.}}$	–	–		2.112
$M_{D_s, 1\text{st}}$	2.313	2.267 <sup>#</sup>							
$M_{\eta_c, \text{g.s.}}$	2.984	2.944 <sup>#</sup>		2.984	$M_{J/\psi, \text{g.s.}}$	3.136	3.098 <sup>#</sup>		3.097
$M_{\eta_c, 1\text{st}}$	3.278		3.225 <sup>#</sup>		$M_{J/\psi, 1\text{st}}$	3.346		3.309 <sup>#</sup>	
$M_{\eta_c, 2\text{nd}}$	3.557	3.508 <sup>#</sup>		3.639	$M_{J/\psi, 2\text{nd}}$	3.593	3.553 <sup>#</sup>		3.686
					$M_{J/\psi, 3\text{rd}}$	3.601	3.563 <sup>#</sup>		3.773

TABLE I: Mass spectrum of pseudo-scalar ( $J^P = 0^-$ ) and vector ( $J^P = 1^-$ ) bound states for the parameter set  $\omega = 0.5 \text{ GeV}$ ,  $D = 16 \text{ GeV}^{-2}$ ,  $m_u = m_d = 5 \text{ MeV}$ ,  $m_s = 115 \text{ MeV}$  and  $m_c = 1130 \text{ MeV}$  and experimental values, in units of GeV. “g.s.”, “1st” and “2nd” etc. stand for ground state, the first and second excitations etc. Gray values marked with \* indicate that calculations already reached the pole region. The “–” for the  $D$ ,  $D^*$  and  $D_s^*$  ground states means that no bound state for the employed parameters could be found; accordingly, there is also no solution for the (radial) excitations. Note for  $D_s$  and  $c\bar{c}$  states the different schemes in fixing the quark masses compared to [19], where  $m_s = 90 \text{ MeV}$  and  $m_c = 1110 \text{ MeV}$  are used (marked by <sup>#</sup>). Experimental data from [42].

can not make an analog analysis of orbital Regge trajectories. Instead, we consider the excitations in the  $0^-$  and  $1^-$  channels separately as a generalization of radial Regge trajectories.

As already mentioned above, here, another issue is the discrepancy of calculated and experimental values of excitations. Another problem is given by the very few excitations which are accessible without intruding poles in the relevant complex momentum domain. In Table I, the states which are hampered by such poles are marked by “\*”. Furthermore, determining the bound states by the zeros of  $\det|\hat{S} - \mathbb{1}|$  does not strictly ensure a given  $\mathcal{C}$  parity. Comparing with [19] one observes some states are to be attributed to  $J^{PC} = 0^{--}$  and  $J^{PC} = 1^{-+}$ , see third columns in Table I in the  $0^-$  and  $1^-$  parts. Instead of disputing the issue of exotic [19] or anomalous states (cf. paragraph 3 in [45] for a comprehensive discussion as well as [46]), we take our calculated values of  $0^-$  and  $1^-$  states and check the arising sequence of g.s. and 1<sup>st</sup>, 2<sup>nd</sup>  $\dots$  states as proxy for radial Regge trajectories for linearity, see Fig. 4 for an example with apparently  $\tilde{n}$  linear trajectory. In fact, for certain parameter choices we find such linear Regge trajectories of excitations parameterized by  $M^2 = M_0^2 + \beta\tilde{n} + c\tilde{n}^2$  with negligibly small values of  $c$ . We ignore thereby

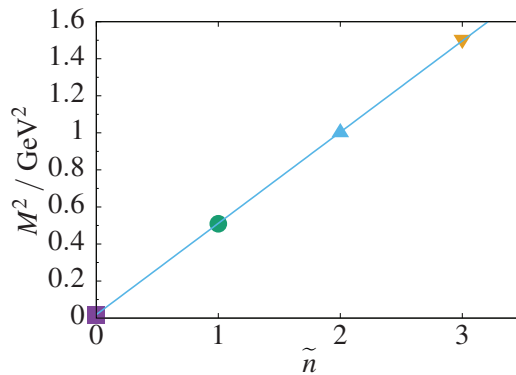


FIG. 4: (Color online) Examples of pion bound states (symbols,  $m_{1,2} = m_q = m_u$ ) and the fitted Regge trajectory (blue line) as a function of the "radial quantum number"  $\tilde{n}$  (which is however a count label for the zeros of  $\det|\hat{S} - \mathbb{1}|$ ) for  $\omega = 0.32 \text{ GeV}$  and  $a = 0.5 \text{ GeV}^3$ . In contrast to our standard parameters used in Table I, here the  $\tilde{n} = 1, 2$  states are shifted and an  $\tilde{n} = 3$  pion state appears additionally.

that some states have improper  $\mathcal{C}$  parity, i.e. we simply attribute the quantity  $\tilde{n}$  to the count label of the excited  $0^-$  or  $1^-$  states as indicated in Table I.

Some survey is exhibited in Fig. 5, where a few  $0^-$  states are depicted (left column) and the Regge slope parameters as well as a linearity measure are displayed too (right column). In that study, we freeze in  $a = \omega^5 D$  and vary the parameter  $\omega$ . As known, the ground state masses are kept constant under such a variation, but evidently the excited states depend on  $\omega$ , even up to a disappearance of certain states, e.g.  $\pi$  and  $\bar{s}s$ . The slope changes with  $\omega$ , while the linearity is strikingly good in the depicted parameter range. This is in contrast to the  $1^-$  channel (see Fig. 6) where, at fixed values of  $\omega^5 D$ , also the ground states vary with changing  $\omega$ ; linear Regge trajectories are hardly accessible within the preferred parameter range adjusted to  $0^-$  states, cf. also [33]. One reason is the appearance of very narrow states, similar to the 3rd/4th excitations in Fig. 2. The other reason is the large nonlinearity measure in some cases or both obstacles together, see Fig. 6. Nevertheless, when taking the averaged energy of the narrow double states and count these as one state, we do see some Regge type behavior for certain parameter ranges.

Despite the poor agreement of (radial) excitations with experimental data, evidenced in Table I in both the  $0^-$  and  $1^-$  channels, we emphasize the occurrence of the linear (Regge) trajectories w.r.t. the count label  $\tilde{n}$  as proxy of the proper radial quantum number  $n$  in the pseudo-scalar channels, thus extending the analysis of [18, 44] towards radial excitations. It remains to be checked whether the Marris-Tandy kernel helps improving the excitations in the vector channel towards establishing a linear Regge pattern, at least qualitatively.

#### IV. SUMMARY

In summary we test the capability to catch the first excited states of mesons (pseudo-scalar  $J^P = 0^-$  and vector  $J^P = 1^-$  channels) by using the Dyson-Schwinger and Bethe-Salpeter equations in rainbow-ladder approximation equipped with the Alkofer-Watson-Weigel kernel. In particular, we establish a certain

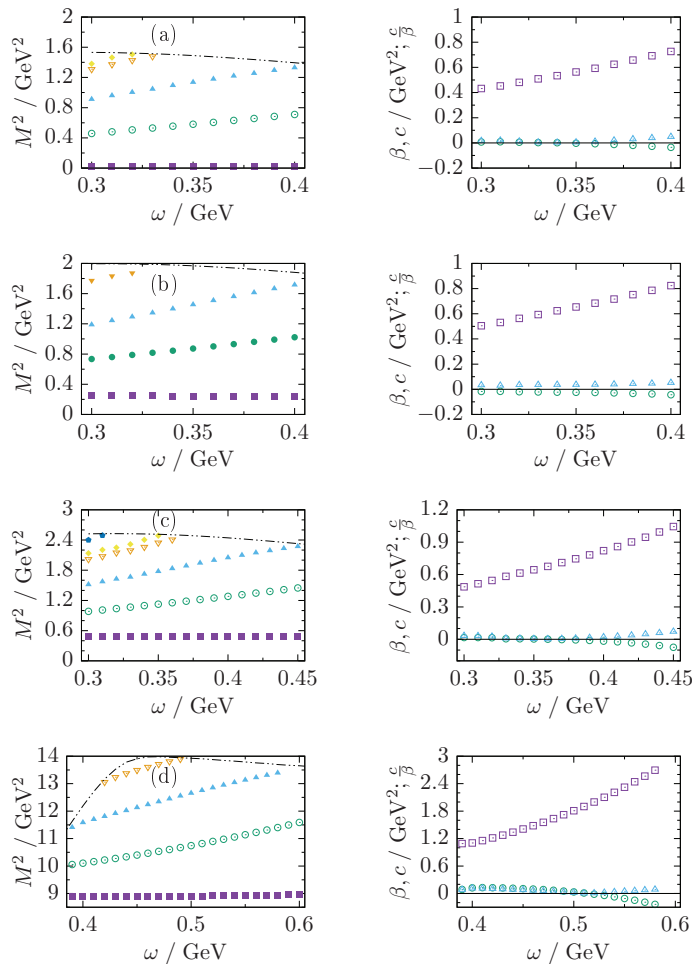


FIG. 5: (Color online) Left column: Spectra of  $0^-$  states representing pions (a:  $m_q = m_u$ ), kaons (b:  $m_1 = m_u$ ,  $m_2 = m_s$ ), fictitious pseudo-scalar  $\bar{s}s$  states (c:  $m_q = m_s$ ), and  $\eta_c$  (d:  $m_q = m_c$ ) as a function of  $\omega$  for  $a \equiv \omega^5 D = 0.5 \text{ GeV}^3$ . The dot-dot-dashed curves mark the limit of the mass squared region wherein a save determination without accounting for divergences is possible. Note the according disappearance of the  $\tilde{n} = 3$  excitations in (a - c) for larger values of  $\omega$  at given  $a$ . The case of  $a = 1 \text{ GeV}^3$  is reported in [41], where also the (dis)appearance regions of  $D$  and  $D_s$  are explored. Empty symbols: exotic states. Right column: The corresponding Regge slope coefficients  $\beta$  (empty violet squares), the quadratic term  $c$  (empty green circles) in fits of the spectra by  $M_n^2 = M_0^2 + \beta \tilde{n} + c \tilde{n}^2$ ,  $\beta \equiv \mu^2$ , and the deviation measure from linear behavior defined by  $|c/\beta|$  (blue triangles).

parameter range in which excitations do form a linear (Regge) trajectory. This is, however, restricted to the pseudo-scalar channel. Other channels, including larger angular momenta, require improvements, among them refined interaction kernels in conjunction with symmetry preserving truncations. The ultimate goal is to arrive a coherent framework which catches the observed sequences of hadron states on Regge trajectories in both the  $J$  and  $n$  directions. This is the first step of an attempt to describe hadron properties, and thus implicitly confinement and relevant scales, together with the subsequent extension to finite temperatures and baryon densities in follow-up investigations. Irrespectively of the quest for



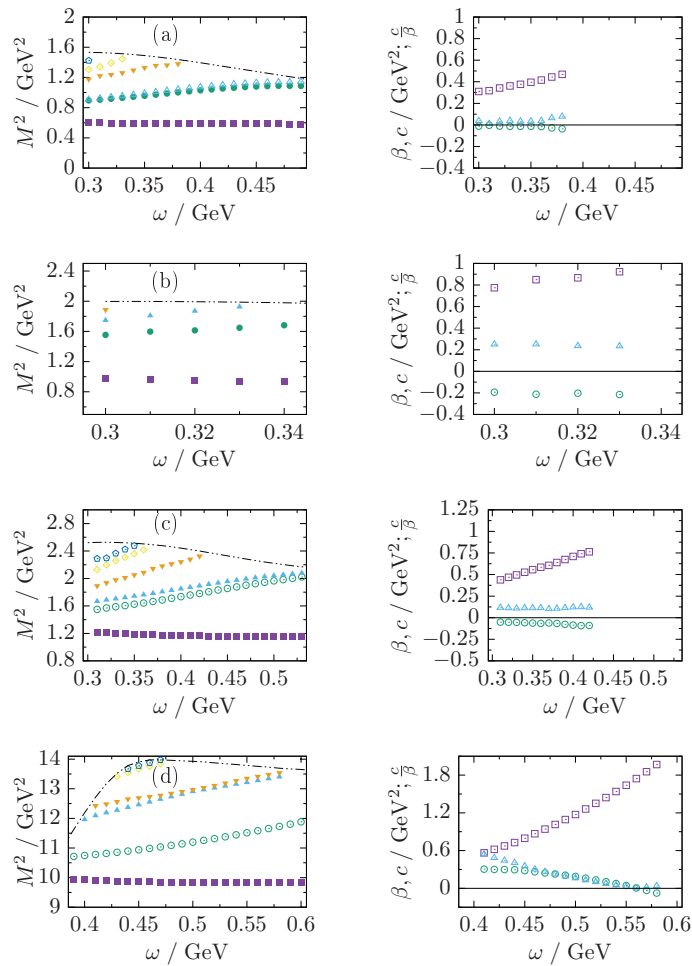


FIG. 6: (Color online) As Fig. 5 but for the  $1^-$  vector channel representing  $\rho$  (a:  $m_q = m_u$ ),  $K^*$  (b:  $m_1 = m_u$ ,  $m_2 = m_s$ ),  $\phi$  (c:  $m_q = m_s$ ), and  $J/\psi$  (d:  $m_q = m_c$ ). Note that in the case of very adjacent states these are handled as one state with averaged energy.

linear Regge trajectories in radial direction is the need of a proper account of the  $1s$ ,  $2s$  and  $3s$  states in the quarkonia vector channels  $J/\psi$  and  $\Upsilon$  which serve as sources of direct probes in ultra-relativistic heavy-ion collisions. According to our contemporary understanding, at some temperature and at small baryon density, hadrons as quasi-particle degrees of QCD should disappear in favor of quasi-quark and quasi-gluon degrees of freedom. The transition happens gradually and may depend on the flavor channel under consideration. For larger baryon densities, the transition could be abrupt, supposed a critical point occurs in the phase diagram of strongly interacting matter. A few large-scale heavy-ion experiments, e.g. the beam-energy scan at RHIC, NA61/SHINE at SPS, CBM at SIS100, as well at NICA and J-PARC address in their physics programs the critical point search. For that, both the properties of hadrons as individual entities and the behavior of hadron matter are key quantities in reconstructing the final state of strong-interaction matter in collision.

### Acknowledgments

The authors gratefully acknowledge the collaboration with S. M. Dorkin, T. Hilger and M. Viebach on the topic.

### Appendix: Spin-angular harmonics

The BS vertex function  $\Gamma$  can be expanded into spin-angular harmonics:

$$\Gamma(p) = \sum_{\alpha=1}^{\alpha_{max}} \Gamma_{\alpha}(p) = \sum_{\alpha=1}^{\alpha_{max}} g_{\alpha}(p) \mathcal{T}_{\alpha}(\vec{p}) \quad (7)$$

with functions  $g_{\alpha}$  fulfilling the orthogonality relation  $g_{\alpha}(p) = \int d\Omega_{\vec{p}} \text{Tr}[\Gamma(p) \mathcal{T}_{\alpha}^{\dagger}(\vec{p})]$ . For pseudo-scalar mesons ( $J^P = 0^{-}$ ), the number of independent spin-angular harmonics  $\alpha_{max} = 4$ , and the set is chosen as

$$\begin{aligned} \mathcal{T}_1(\vec{p}) &= \frac{1}{\sqrt{16\pi}} \gamma^5 = \mathcal{T}_1^{\dagger}(\vec{p}), & \mathcal{T}_2(\vec{p}) &= \frac{1}{\sqrt{16\pi}} \gamma^0 \gamma^5 = -\mathcal{T}_2^{\dagger}(\vec{p}), \\ \mathcal{T}_3(\vec{p}) &= -\frac{1}{\sqrt{16\pi}} \not{p} \gamma^0 \gamma^5 = \mathcal{T}_3^{\dagger}(\vec{p}), & \mathcal{T}_4(\vec{p}) &= -\frac{1}{\sqrt{16\pi}} \not{p} \gamma^5 = \mathcal{T}_4^{\dagger}(\vec{p}), \end{aligned} \quad (8)$$

and for vector mesons ( $J^P = 1^{-}$ ),  $\alpha_{max} = 8$  with

$$\begin{aligned} \mathcal{T}_1(\vec{p}) &= \sqrt{\frac{1}{16\pi}} \not{\xi}_{\mathcal{M}} = \mathcal{T}_1^{\dagger}(\vec{p}), & \mathcal{T}_2(\vec{p}) &= -\sqrt{\frac{1}{16\pi}} \gamma^0 \not{\xi}_{\mathcal{M}} = \mathcal{T}_2^{\dagger}(\vec{p}), \\ \mathcal{T}_3(\vec{p}) &= -\sqrt{\frac{3}{16\pi}} (n_{\vec{p}} \xi_{\mathcal{M}}) = \mathcal{T}_3^{\dagger}(\vec{p}), \\ \mathcal{T}_4(\vec{p}) &= \sqrt{\frac{3}{32\pi}} \gamma^0 [-(n_{\vec{p}} \xi_{\mathcal{M}}) + \not{p} \not{\xi}_{\mathcal{M}}] = -\mathcal{T}_4^{\dagger}(\vec{p}), \\ \mathcal{T}_5(\vec{p}) &= \sqrt{\frac{1}{32\pi}} [\not{\xi}_{\mathcal{M}} + 3(n_{\vec{p}} \xi_{\mathcal{M}}) \not{p}] = -\mathcal{T}_5^{\dagger}(\vec{p}), \\ \mathcal{T}_6(\vec{p}) &= \sqrt{\frac{1}{32\pi}} \gamma^0 [\not{\xi}_{\mathcal{M}} + 3(n_{\vec{p}} \xi_{\mathcal{M}}) \not{p}] = \mathcal{T}_6^{\dagger}(\vec{p}), \\ \mathcal{T}_7(\vec{p}) &= -\sqrt{\frac{3}{16\pi}} \gamma^0 (n_{\vec{p}} \xi_{\mathcal{M}}) = \mathcal{T}_7^{\dagger}(\vec{p}), \\ \mathcal{T}_8(\vec{p}) &= \sqrt{\frac{3}{32\pi}} [-(n_{\vec{p}} \xi_{\mathcal{M}}) + \not{p} \not{\xi}_{\mathcal{M}}] = -\mathcal{T}_8^{\dagger}(\vec{p}). \end{aligned} \quad (9)$$

Scalar products are displayed here in Minkowski space;  $n_{\vec{p}}$  is the unit vector  $n_{\vec{p}} = (0, \vec{p}/|\vec{p}|)$ ,  $\xi_{\mathcal{M}} = (0, \vec{\xi}_{\mathcal{M}})$  is the polarization vector fixed by  $\vec{\xi}_{+1} = -(1, i, 0)/\sqrt{2}$ ,  $\vec{\xi}_{-1} = (1, -i, 0)/\sqrt{2}$ ,  $\vec{\xi}_0 = (0, 0, 1)$  and slashed quantities such as  $\not{x}$  represent  $\gamma^{\mu} x_{\mu}$ .

The partial amplitudes  $\Gamma_{\alpha}(p)$  and the interaction kernel (6) are decomposed over the basis of spherical harmonics  $Y_{lm}(\theta, \phi)$  and normalized Gegenbauer polynomials  $X_{nl}(\chi)$ ,

$$Z_{nlm} = X_{nl}(\chi) Y_{lm}(\theta, \phi) \quad (10)$$

$$= \sqrt{\frac{2^{2l+1}}{\pi} \frac{(n+1)(n-l)!!^2}{(n+l+1)!}} \sin^l \chi G_{n-l}^{l+1}(\cos \chi) Y_{lm}(\theta, \phi), \quad (11)$$

with familiar Gegenbauer polynomials  $G_{n-l}^{l+1}(\cos \chi)$ . The hyper angle  $\chi$  is defined by  $\cos \chi = p_4/\tilde{p}$  and  $\sin \chi = |\vec{p}|/\tilde{p}$ , where  $\tilde{p} = (p_4^2 + \vec{p}^2)^{1/2}$  is the modulus for an Euclidean four-vector  $p = (p_4, \vec{p})$ . The partial decompositions of  $\Gamma_\alpha(p)$  and  $D^{AWW}(p-k)$  read

$$\Gamma_\alpha(p) = \sum_n \varphi_{\alpha, l_\alpha}^n(\tilde{p}) X_{nl_\alpha}(\chi_p) \mathcal{T}_\alpha(\vec{p}), \quad (12)$$

$$D^{AWW}(p-k) = 2\pi^2 \sum_{\kappa\lambda\mu} \frac{1}{\kappa+1} V_\kappa(\tilde{p}, \tilde{k}) X_{\kappa\lambda}(\chi_p) X_{\kappa\lambda}(\chi_k) Y_{\lambda\mu}(\Omega_p) Y_{\lambda\mu}^*(\Omega_k), \quad (13)$$

where  $V_\kappa(\tilde{p}, \tilde{k})$  are the partial kernels and  $\varphi_{\alpha, l_\alpha}^n(\tilde{p})$  are the expansion coefficients of the partial amplitudes. Actually  $l_\alpha$  is restricted by the corresponding orbital momentum encoded in  $\mathcal{T}_\alpha(\vec{p})$ . For  $\mathcal{T}_{1,2}(\vec{p})$  from Eq. (8),  $l_\alpha = 0$  holds, while for  $\mathcal{T}_{3,4}(\vec{p})$   $l_\alpha = 1$ . In analogy for vector mesons (see (9)),  $l_\alpha = 0$  for  $\mathcal{T}_{1,2}(\vec{p})$ ,  $l_\alpha = 1$  for  $\mathcal{T}_{3,4,7,8}(\vec{p})$  and  $l_\alpha = 2$  for  $\mathcal{T}_{5,6}(\vec{p})$ .

The spin-angular harmonics  $\mathcal{T}_\alpha(\vec{p})$  possess a well defined  $\mathcal{C}$  parity, and the normalized Gegenbauer polynomials  $X_{nl}(\chi_p)$  have a well defined symmetry too. Therefore, keeping only each second entry in the sum in Eq. (12) yields a well defined  $\mathcal{C}$  parity of the bound states upon  $\bar{\Gamma}(q, P) \equiv [\mathcal{C} \Gamma(-q, P) \mathcal{C}^{-1}]^T = \eta_C \Gamma(q, P)$  with  $\mathcal{C} = \gamma_2 \gamma_4$  (see [19] for further details).

Changing the integration variables to the hyperspace,  $d^4k = \tilde{k}^3 \sin^2 \chi_k \sin \theta_k d\tilde{k} \times d\chi_k d\theta_k d\phi_k$ , inserting Eq. (12) and (13) into (5) and performing the necessary angular integration, a system of integral equations for the expansion coefficients  $\varphi_{\alpha, l_\alpha}^n(\tilde{p})$  as the  $N$  elements of  $X$  remains:

$$\varphi_{\alpha, l_\alpha}^n(\tilde{p}) = \sum_\beta \sum_{m=1}^{\infty} \int d\tilde{k} \tilde{k}^3 \hat{S}_{\alpha\beta}(\tilde{p}, \tilde{k}, m, n) \varphi_{\beta, l_\beta}^m(\tilde{k}). \quad (14)$$

The explicit expression for  $\hat{S}_{\alpha\beta}(\tilde{p}, \tilde{k}, m, n)$  reads

$$\begin{aligned} \hat{S}_{\alpha\beta}(\tilde{p}, \tilde{k}, m, n) &= \sum_\kappa \int \sin^2 \chi_k d\chi_k X_{m l_\beta}(\chi_k) X_{\kappa\lambda}(\chi_k) \sigma_{s,v}(\tilde{k}_1^2) \sigma_{s,v}(\tilde{k}_2^2) \\ &\times A_{\alpha\beta}(\tilde{p}, \tilde{k}, \kappa, \chi_k, n), \end{aligned} \quad (15)$$

where  $\tilde{k}_{1,2}^2$  is given by  $\tilde{k}_{1,2}^2 = \tilde{k}^2 - \eta_{1,2}^2 M_{12}^2 \pm \eta_{1,2} M_{12} \cos \chi$  with momentum partitioning parameters  $\eta_1 + \eta_2 = 1$  and  $A_{\alpha\beta}(\tilde{p}, \tilde{k}, \kappa, \chi_k, n)$  results from calculations of traces and angular integrations as

$$\begin{aligned} A_{\alpha\beta}(\tilde{p}, \tilde{k}, \kappa, \chi_k, n) &= \int \sin^2 \chi_p d\chi_p d\Omega_p d\Omega_k V_\kappa(\tilde{p}, \tilde{k}) X_{nl_\alpha}(\chi_p) X_{\kappa\lambda}(\chi_p) Y_{\lambda\mu}(\Omega_p) Y_{\lambda\mu}^*(\Omega_k) \\ &\times \text{Tr}[d_{\mu\nu}((p-k)^2) \gamma^\mu \dots \mathcal{T}_\alpha(\vec{p}) \dots \mathcal{T}_\alpha(\vec{p}) \gamma^\nu]. \end{aligned} \quad (16)$$

- 
- [1] Z. Yang, Q. Wang and U. G. Meissner, Phys. Lett. B **767** (2017) 470.
  - [2] A. V. Anisovich, V. V. Anisovich and A. V. Sarantsev, Phys. Rev. D **62** (2000) 051502.
  - [3] P. Masjuan, E. Ruiz Arriola and W. Broniowski, Phys. Rev. D **85** (2012) 094006.
  - [4] P. Masjuan, E. Ruiz Arriola and W. Broniowski, Phys. Rev. D **87** (2013) 118502.
  - [5] E. Klempt and A. Zaitsev, Phys. Rept. **454** (2007) 1.
  - [6] S. J. Brodsky, G. F. de Teramond, H. G. Dosch and J. Erlich, Phys. Rept. **584** (2015) 1.
  - [7] D. V. Bugg, Phys. Rev. D **87** (2013) 118501.

- [8] D. V. Bugg, Phys. Rept. **397** (2004) 257.
- [9] S. S. Afonin, Eur. Phys. J. A **29** (2006) 327.
- [10] S. S. Afonin and I. V. Pusenkov, EPJ Web Conf. **125** (2016) 04006.
- [11] D. Ebert, R. N. Faustov and V. O. Galkin, Eur. Phys. J. C **66** (2010) 197.
- [12] D. Ebert, R. N. Faustov and V. O. Galkin, Phys. Rev. D **79** (2009) 114029.
- [13] S. S. Afonin, Phys. Lett. B **675** (2009) 54.
- [14] S. S. Afonin, Phys. Lett. B **678** (2009) 477.
- [15] D. Li and M. Huang, JHEP **1311** (2013) 088.
- [16] D. Li, M. Huang and Q. S. Yan, Eur. Phys. J. C **73** (2013) 2615.
- [17] R. Zöllner and B. Kämpfer, J. Phys. Conf. Ser. **1024** (2018) 012003.
- [18] C. S. Fischer, S. Kubrak and R. Williams, Eur. Phys. J. A **50** (2014) 126.
- [19] T. Hilger, M. Gomez-Rocha, A. Krassnigg and W. Lucha, Eur. Phys. J. A **53** (2017) 213.
- [20] D. Binosi, L. Chang, J. Papavassiliou, S. X. Qin and C. D. Roberts, Phys. Rev. D **93** (2016) 096010.
- [21] K. I. Wang, Y. x. Liu, L. Chang, C. D. Roberts and S. M. Schmidt, Phys. Rev. D **87** (2013) 074038.
- [22] H. Suganuma, T. M. Doi, K. Redlich and C. Sasaki, J. Phys. G **44** (2017) 124001.
- [23] A. M. Sirunyan *et al.* [CMS Collaboration], Phys. Lett. B **790**, 270 (2019).
- [24] M. Aaboud *et al.* [ATLAS Collaboration], Eur. Phys. J. C **78**, no. 9, 762 (2018)
- [25] A. M. Sirunyan *et al.* [CMS Collaboration], Phys. Lett. B **790**, 509 (2019).
- [26] A. M. Sirunyan *et al.* [CMS Collaboration], Phys. Rev. Lett. **120**, no. 14, 142301 (2018).
- [27] S. Aronson, E. Borrás, B. Odegard, R. Sharma and I. Vitev, Phys. Lett. B **778**, 384 (2018).
- [28] R. Alkofer, P. Watson and H. Weigel, Phys. Rev. D **65** (2002) 094026.
- [29] S. M. Dorkin, M. Viebach, L. P. Kaptari and B. Kämpfer, J. Mod. Phys. **7** (2016) 2071.
- [30] S. M. Dorkin, L. P. Kaptari and B. Kämpfer, Phys. Rev. C **91** (2015) 055201.
- [31] S. M. Dorkin, L. P. Kaptari, T. Hilger and B. Kämpfer, Phys. Rev. C **89** (2014) 034005.
- [32] S. M. Dorkin, T. Hilger, L. P. Kaptari and B. Kämpfer, Few Body Syst. **49** (2011) 247.
- [33] F. F. Mojica, C. E. Vera, E. Rojas and B. El-Bennich, Phys. Rev. D **96** (2017) 014012.
- [34] B. El-Bennich, G. Krein, E. Rojas and F. E. Serna, Few Body Syst. **57** (2016) 955.
- [35] A. Holl, A. Krassnigg and C. D. Roberts, Phys. Rev. C **70** (2004) 042203.
- [36] A. Holl, A. Krassnigg, P. Maris, C. D. Roberts and S. V. Wright, Phys. Rev. C **71** (2005) 065204.
- [37] S. x. Qin, L. Chang, Y. x. Liu, C. D. Roberts and D. J. Wilson, Phys. Rev. C **85** (2012) 035202.
- [38] E. Rojas, B. El-Bennich and J. P. B. C. de Melo, Phys. Rev. D **90** (2014) 074025.
- [39] T. Hilger, M. Gomez-Rocha and A. Krassnigg, Eur. Phys. J. C **77** (2017) 625.
- [40] P. Maris and P. C. Tandy, Phys. Rev. C **60** (1999) 055214.
- [41] R. Greifenhagen, Investigation of the AWW kernel for describing the excited meson spectrum in a combined Dyson-Schwinger – Bethe-Salpeter approach, Master Thesis, TU Dresden (2016).
- [42] M. Tanabashi *et al.* (Particle Data Group), Phys. Rev. D **98** (2018) 030001.
- [43] T. Hilger and A. Krassnigg, Eur. Phys. J. A **53** (2017) 142.
- [44] S. Kubrak, C. S. Fischer and R. Williams, J. Phys. Conf. Ser. **599** (2015) 012013.
- [45] G. Eichmann, Few Body Syst. **58**, no. 2, 81 (2017)
- [46] S. Ahlig and R. Alkofer, Annals Phys. **275**, 113 (1999)